biomedicines

MDPI

Article

Phagocytic Function Analyses of GAB_BR-Related Microglia in Immature Developing Epileptic Brain Based on 10× Single-Nucleus RNA Sequencing Technology

Yunhao Gan [1,2], Xiaoyue Yang [1,2], Tianyi Li [1,2], Ziyao Han [1,2], Li Cheng [1,2], Lingling Xie [1,2,*] and Li Jiang [1,2,*]

[1] Department of Neurology, Children's Hospital of Chongqing Medical University, National Clinical Research Center for Child Health and Disorders, Ministry of Education Key Laboratory of Child Development and Disorders, Chongqing 400014, China; yunhaogan28@163.com (Y.G.); yangxiaoyue97@163.com (X.Y.); litianyihka@126.com (T.L.); ziyaohan0410@163.com (Z.H.); 480867@hospital.cqmu.edu.cn (L.C.)

[2] Chongqing Key Laboratory of Child Neurodevelopment and Cognitive Disorders, Chongqing Medical University, Chongqing 400014, China

* Correspondence: lingling_xie@hospital.cqmu.edu.cn (L.X.); dr_jiangcqmu@163.com (L.J.)

Abstract: Background: Epilepsy is a neurological disorder defined by the occurrence of epileptic seizures, which can significantly affect children, often leading to learning and cognitive impairments. Microglia, the resident immune cells of the central nervous system, are essential in clearing damaged neurons through phagocytosis. Notably, GAB_BR-associated microglia have been implicated in regulating phagocytic activity. Since the phagocytic function of microglia is critical in the pathogenesis of epilepsy, this study aims to investigate the role of GAB_BR-associated microglia in the development of the immature brain following epileptic seizures. **Methods:** Epilepsy was induced in a mouse model by the intraperitoneal injection of KA. Changes in the expression of the GAB_BR-related gene, GAB_BR2, in hippocampal microglia were analyzed using single-nucleus RNA sequencing (snRNA-seq). Cognitive and emotional changes in the mice were assessed through behavioral analyses. The expression of GAB_BR2 was semi-quantitatively measured using Western blotting, quantitative reverse transcription PCR, and immunofluorescence. Additionally, the spatial relationship between GAB_BR2 and hippocampal neurons was evaluated using Imaris software. **Results:** The snRNA-seq analysis revealed that GAB_BR2 expression was elevated in activated microglia in the hippocampus during chronic epilepsy compared to the early phase of seizures. Behavioral assessments demonstrated heightened anxiety levels and learning and memory impairments in the chronic epilepsy group compared to the control group. GAB_BR2 expression was upregulated in chronic epilepsy. Three-dimensional reconstruction analyses revealed a significantly increased contact volume between GAB_BR-associated microglia and neurons in the chronic epilepsy group compared to the control group. **Conclusions**: GAB_BR-associated microglia significantly contribute to the progression of immature brain diseases by promoting neuronal phagocytic activity.

Keywords: epilepsy; GAB_BR-associated microglia; GAB_BR2; microglia; phagocytic pruning

check for updates

Academic Editors: Natalia V. Gulyaeva and Hua-Jun Feng

Received: 5 January 2025
Revised: 15 January 2025
Accepted: 18 January 2025
Published: 22 January 2025

Citation: Gan, Y.; Yang, X.; Li, T.; Han, Z.; Cheng, L.; Xie, L.; Jiang, L. Phagocytic Function Analyses of GAB_BR-Related Microglia in Immature Developing Epileptic Brain Based on 10× Single-Nucleus RNA Sequencing Technology. *Biomedicines* **2025**, *13*, 269. https://doi.org/10.3390/biomedicines13020269

Copyright: © 2025 by the authors. Licensee MDPI, Basel, Switzerland. This article is an open access article distributed under the terms and conditions of the Creative Commons Attribution (CC BY) license (https://creativecommons.org/licenses/by/4.0/).

1. Introduction

In recent years, the prevalence of epilepsy among children and adolescents has steadily increased. Abnormal and excessively synchronized neuronal activity in the brain often results in poor prognoses and elevated mortality rates [1–3]. Although various antiepileptic drugs (AEDs) can mitigate and control seizures, these treatments are frequently associated with significant side effects and resistance, posing considerable safety concerns [4–6].

Epilepsy is a chronic neurological disorder characterized by recurrent, transient brain dysfunction caused by abnormal neuronal discharges, leading to repeated seizures.

In infants and young children, seizures represent one of the most common neurological emergencies, with approximately 5% of children experiencing such episodes [5,7]. Status epilepticus (SE), a severe and prolonged seizure, affects 17–23 per 100,000 children and carries a mortality rate of 16%. Current treatments primarily rely on AEDs and acute antispasmodic medications [7]. However, despite the availability of various AEDs, approximately 20% of pediatric epilepsy cases remain difficult to manage. Therefore, the development of novel therapeutic strategies to treat pediatric epilepsy and protect the developing brain is imperative.

Extensive research has primarily focused on the abnormal neurophysiological processes of epileptic neurons, yet the phagocytic activity of microglia in clearing synapses and dead neurons is equally critical in epilepsy pathogenesis [8–10]. Investigating the role of microglial phagocytosis may offer valuable insights into the mechanisms underlying epilepsy. Previous studies have demonstrated that knocking out TREM2 in epilepsy models reduces microglial proliferation and impairs their ability to clear damaged hippocampal neurons [11]. This reduction in the selective phagocytosis of inhibitory synapses by microglia may disrupt the balance of excitatory and inhibitory (E/I) neurotransmission, thereby contributing to seizure development and symptom severity [12]. Despite these findings, the regulatory mechanisms governing microglial phagocytosis in the brain remain poorly understood.

Gamma-aminobutyric acid (GABA) serves as the primary inhibitory neurotransmitter in the central nervous system, mediating inhibitory synaptic signaling through interactions with GAB_B receptors (GAB_BR) [13,14]. As a G protein-coupled receptor, GAB_BR induces neuronal hyperpolarization and reduces presynaptic neurotransmitter release by regulating potassium (K^+) levels and inhibiting calcium (Ca^{2+}) release [2,15]. Research has demonstrated that microglia express a significant amount of GAB_BR, which plays a critical role in modulating immune responses in the brain through GABA signaling [16–18]. Despite these findings, the specific role of GAB_BR-associated microglia in the development of epilepsy in the immature brain remains poorly understood.

We established an epilepsy model through intraperitoneal injection of kainic acid (KA), which induces SE and leads to spontaneous recurrent seizures (SRSs) during the chronic phase of epilepsy [19]. Our findings revealed that KA-induced epileptic mice exhibited significant cognitive impairments in the chronic epilepsy stage. Furthermore, microglia associated with GAB_BR demonstrated an enhanced capacity to phagocytose damaged hippocampal neurons. Collectively, these results suggest that GAB_BR-associated microglia may play a pivotal role in neuronal phagocytosis in developmental epilepsy and represent a potential therapeutic target for early intervention and the treatment of epilepsy.

2. Materials and Methods

2.1. Animals

In this study, fourteen-day-old male C57BL/6 mice, sourced from the Laboratory Animal Center of Chongqing Medical University, Chongqing, China, were housed collectively in our SPF facility and subjected to a 12 h light/dark cycle, with ad libitum access to food and water. In this study, no more than five mice were housed per cage. Ethical approval for all procedures was granted by the Commission of Chongqing Medical University for Ethics of Experiments on Animals, and all were conducted in compliance with international standards. All procedures for this study were approved by the Animal Care and Committee of Chongqing Medical University (Approval number: IACUC-CQMU-2024-0639). The experimental design was both randomized and double-blind, involving immature

developing mice aged P14. Efforts were made to minimize animal suffering and to reduce the number of animals used throughout the experiments.

2.2. Kainic Acid (KA) Model of Epilepsy

The intraperitoneal (i.p.) administration of KA to induce status epilepticus (SE) was established using a previously described method [20]. Ninety-six mice were administered a single dose of KA (0.75 μL/g, Sigma–Aldrich, St. Louis, MO, USA), resulting in continuous SE for 30 min, followed by the administration of 1 mg/kg (i.p.) diazepam to terminate the condition. Seizure severity was assessed using Racine's scale: stage 0, no response or behavior arrest; stage 1, chewing or facial twitches; stage 2, chewing and head nodding or wet dog shakes; stage 3, unilateral forelimb clonus; stage 4, bilateral forelimb clonus and rearing; stage 5, bilateral forelimb clonus, rearing, and falling [21].

In this investigation, the majority of mice exhibited SE at stages 3–5, with an approximate mortality rate of 20%. The control group, comprising eighty-seven mice, received solely 0.1% phosphate-buffered saline (PBS) and diazepam. The experimental groups were designated as the 14-1-SC group, 14-7-SC group, 14-14-SC group, and 14-28-SC group. Correspondingly, the control groups were named the 14-1-Control group, 14-7-Control group, 14-14-Control group, and 14-28-Control group, respectively.

2.3. Reagents and Antibodies

The following antibodies were used: IBA1 and NeuN were from Novus and Pronteintech, respectively (Cat# NB100-1028, Littleton, CO, USA, RRID: AB_3148646; Cat# 66836-1-Ig, Wuhan, China, RRID: AB_2880708). Antibodies against GAB_BR2 for immunofluorescence (IF) and Western blot (WB) analysis came from Santacruz (Cat# sc-393286, CA, USA, RRID: AB_3668753). Antibodies against β-actin for WB came from Proteintech (Cat# HRP-60008, Proteintech, Wuhan, China, RRID: AB_2722565). Donkey anti-rabbit, Donkey anti-mouse and Donkey anti-goat secondary antibodies and hydrochloric acid (DAPI) were purchased from Thermo Fisher (A10042, A-31571, A-11055, 62247, Waltham, MA, USA).

2.4. Immunostaining, Imaging, and Quantification

This study utilizes frozen sections for immunofluorescence staining, as previously outlined in reference [22]. The slices were washed three times with PBS, permeated, and blocked using a solution containing 5% BSA and 0.1% Triton X-100 (CAS 9036-19-5; Sigma-Aldrich, St. Louis, MO, USA) at room temperature for one hour. Subsequently, the tissue slices were incubated with the primary antibody in a blocking solution overnight at 4 °C. Following multiple washes, the blocking solution was augmented with the secondary antibody containing DAPI and incubated for 1 h. Images were acquired using an Olympus microscope (VS200, Spin SR, Tokyo, Japan). To determine the cellular localization of GAB_BR2, 3 random images were captured from different fields within the same region using a 60× oil immersion microscope. The staining intensity of GAB_BR2-positive microglia was quantified using Image J. Each brain cell was delineated as an individual region of interest (ROI), and the mean pixel density was calculated [23].

2.5. Three-Dimension (3D) Reconstruction and Quantification

The quantitative phagocytosis method was described previously [23]. For 3D reconstruction, 20 μm confocal stacks were analyzed with Imaris software (version 9.0.1, Bitplane). High-resolution confocal images were subjected to 3D reconstruction to visualize GABBR2-positive microglia, employing co-staining with IBA1, GABBR2, and NeuN. Subsequently, the reconstructed surface volume of IBA1-engulfing NeuN was recorded and analyzed.

2.6. Single-Nucleus RNA-Seq

The original Fastq files for the 14-1-Control, 14-1-SC, 14-28-Control, and 14-28-SC mouse hippocampus datasets were generated using 10× Genomics technology for library preparation, quality control, and sequencing. The raw data files were processed with Cell Ranger v7.1.0 software for subsequent analysis. Seurat (version 4.0.5) was employed to load the processed data for each dataset into R individually. Cell quality was assessed based on the following criteria: (1) the total UMI count (library size) per cell was less than 30,000; (2) the number of detected genes ranged between 200 and 7000; (3) the percentage of mitochondrial gene expression was below 5%; and (4) cells with more than 200 detected genes were selected for further analysis. Doublets were removed using the default settings of DoubletFinder for each sample. The number of primitive cells in the 14-1-Control, 14-1-SC, 14-28-Control, and 14-28-SC mouse hippocampal datasets were 12,488, 12,924, 12,392, and 14,911, respectively. After filtering the cells based on the above parameters, the cell numbers were 10,839, 11,011, 11,718, and 11,177, respectively.

After filtering out low-quality cells, the Integration method in R was used to process and integrate the data with default parameters. Integration involved comparing cells across different batches or experimental conditions based on the "origin.dent" variable. Following the integration of selected anchor points, dimensionality reduction and clustering were performed on the combined dataset to identify cell subpopulations. Cell clusters in each sample were identified by analyzing the top 20 principal components (PCs) of highly variable genes (HVGs).

Seurat's FindAllMarkers function was then employed to identify marker genes for each cell cluster, which were subsequently annotated manually. To classify the major cell lineages, a set of established marker genes from previous studies was utilized. For astrocytes, markers included Glul, Slc1a3, and Aqp4; for microglia, Cx3cr1, Hexb, and P2ry12; for neurons, Map2, Syn3, and Rbfox3; for oligodendrocytes, Mog, Mag, and Mbp; and for endothelial cells, Fn1, Hmcn1, and Cped1.

After identifying the main cell lineages, the Subset function was used to further perform dimensionality reduction and clustering specifically on microglia cells to identify their subpopulations. For resting microglia, marker genes included Cx3cr1, P2ry12, and Tmem119, while for activated microglia, markers such as Apoe, Cd40, and Arg1 were used. In this phase of the experiment, data visualization was conducted using the DimPlot, DotPlot, EigenPlot, and VlnPlot functions, while cell proportions were calculated and displayed using ggplot. Additionally, manual adjustments were applied during this stage to prevent excessive clustering.

2.7. Open Field Test (OTF)

An OFT was conducted in an arena measuring 40 cm × 40 cm × 40 cm. The specific experimental method is as described earlier [24]. In this test, each mouse was positioned at the center of the arena and permitted to explore for a duration of 10 min. Recorded metrics included the average speed and the duration of time spent in the central area. The arena was cleaned with 70% ethanol between mice. The percentage of time spent in the central area was subsequently compared between the two groups. A reduced duration in the central area was indicative of anxiety and depression-like behaviors in the experimental mice.

2.8. Elevated Plus Maze (EPM)

The EPM apparatus comprises four rectangular arms, each measuring 50 cm × 10 cm, connected by a central square platform with dimensions of 10 cm × 10 cm. The apparatus includes two closed arms and two open arms, with the closed arms being enclosed by opaque walls that are 40 cm in height on three sides. During the experimental procedure,

each subject was placed at the central platform and allowed to explore the maze freely for a duration of 5 min. Following the assessment of each subject, the EPM was disinfected using 75% ethanol. Subsequently, the trajectory length, velocity, and duration spent in both the open and closed arms were quantified and analyzed.

2.9. Novel Object Recognition (NOR)

As previously described, an NOR test was conducted in an open field measuring 40 cm × 40 cm × 40 cm [25]. The animals underwent a 5 min training period, during which they were placed in the center of the arena containing two identical objects. Exploratory behavior, defined as the time spent investigating each object, was recorded. After a 24 h interval, the subjects were reintroduced into the arena for the testing phase, during which one of the original objects was replaced with a novel object. The time spent exploring both the familiar and novel objects was measured once again. The results are expressed as the percentage of time spent exploring each object during training or testing.

2.10. Y Maze

All mice were subjected to a Y maze test, as previously described, to assess working memory impairment [26]. The Y maze apparatus consists of three arms, each measuring 30 cm × 6 cm × 15 cm. During the test, a mouse is placed in one arm and permitted to explore all three arms freely for a duration of 8 min. The spontaneous alternation rate is subsequently calculated using software. In the context of the Y-maze test, a reduced alternation rate is indicative of impaired working memory.

2.11. Morris Water Maze (MWM)

An MWM test was conducted, as previously described, in a circular pool with a diameter of 110 cm and a water temperature of 24 °C [27]. The platform, measuring 10 cm in diameter, is submerged 1 cm below the water surface. The test involves placing each mouse at four quadrants' starting positions daily, providing 60 s to locate the platform during a 5-day training experiment. Should the mouse fail to reach the platform within this period, it is then guided to the platform. Once the mouse locates the platform, it is maintained on the platform for 15 s. The escape latency is recorded using software. During the testing day, the platform is removed, and the mice are allowed to swim freely in the pool for 60 s. Relevant memory abilities are quantified using software.

2.12. Western Blot (WB)

The immunoblotting procedure was performed as previously described [28]. Briefly, total protein was extracted using RIPA buffer (RIPA–phosphatase inhibitor cocktail = 100:1) with the addition of 5× loading buffer. Equal amounts of protein were separated on a 10% SDS-polyacrylamide gel and transferred onto a nitrocellulose membrane (GVHP29325, Millipore, Billerica, MA, USA). The membrane was incubated with primary antibodies overnight at 4 °C. The next day, the membrane was incubated with appropriately diluted secondary antibodies for 1 h at room temperature. Protein bands were visualized using a chemiluminescence WB detection reagent (BJ0004A, Biosharp, Hefei, China). The unprocessed image, without WB cropping, is provided in Supplemental Figure S1.

2.13. qRT–PCR (Quantitative Reverse Transcription-Polymerase Chain Reaction)

Total RNA from cultured and tissues was extracted using the FastPure Cell/Tissue Total RNA Isolation Kit (Vazyme Nanjing, China) and reverse-transcribed using the AB-Script III RT Master Mix qPCR with gDNA Remover (ABclonal, Wuhan, China) following the manufacturer's instructions. Real-time PCR was conducted on a Biorad 96 Touch machine (Bio-Rad, Hercules, CA, USA) using the 2× Universal SYBR Green Fast qPCR

Mix (ABclonal, Wuhan, China). β-actin served as the internal control. The cycle threshold (Ct) values of the target gene transcripts were normalized to the average Ct of the housekeeping gene β-actin in each reaction. Relative transcript levels were quantified using the comparative Ct ($^{\Delta\Delta}$Ct) method. Primer sequences for the qRT-PCR analysis are provided below:

GAB_BR2:	Forward: 5′-AGACTCCACAGCAATACGAAAGA-3′
	Reverse: 3′-TTCATGGCGTTGAGGATGATTCT-5′
β-actin:	Forward: 5′-AGTGTGACGTTGACATCCGTA-3′
	Reverse: 3′-GCCAGAGCAGTAATCTCCTTC-5′

2.14. Statistics and Reproducibility

According to previous research [29], the sample size for this experiment was calculated with the formula E = total number of animals in each group, ensuring each experimental design an E value exceeding 10. Following established research guidelines, the significance threshold was established at $\alpha = 0.05$ and the power at 0.80. Consequently, the Wilcoxon Mann–Whitney test determined the minimum effective sample size between the two groups to be N = 3 [30]. This study acknowledges several limitations, including the lack of an initial sample size calculation. However, due to the inherent variability and uncontrollability of the research, a sample size of n = 5 mice was chosen. The most recent iteration of GraphPad Prism 9 (GraphPad Software) was employed for statistical analyses and graphical representations. The Shapiro–Wilk test was utilized to assess the normality of the data distribution. Depending on the results of the normality test, the statistical significance of differences between the two groups was evaluated using either the unpaired two-tailed Student's *t*-test or the Mann–Whitney U test. $p > 0.05$ was considered indicative of statistical significance. All values are presented as the mean ± standard deviation (SD). Non-parametric data are presented as median ± interquartile range.

3. Results

3.1. Integration and Cell Type Identification of Single Nuclear RNA Sequencing Data from Normal and Epilepsy Groups in Immature Developing Brain

In this study, we initially performed cell quality control and data dimensionality reduction on datasets from both the normal and epilepsy groups. Subsequently, we conducted UMAP analysis on each dataset to define cell populations across four datasets (Figure 1A–D). Next, we integrated four sets of snRNA-seq data, applying rigorous cell quality control and data dimensionality reduction. This integration significantly enhanced the diversity and scale of the data, providing a robust foundation for subsequent analyses. This integration significantly enhanced the diversity and scale of the data, providing a robust foundation for subsequent analyses (Figure 1E).

Using the "FindAllMarkers" function in Seurat, we classified the cells into four primary types based on established marker genes [23]. These cell types include microglia, marked by *Cx3cr1*, *Hexb*, and *P2ry12*; neurons, marked by *SYN3*, *Map2*, and *RBFOX3*; myelin-forming glial cells, marked by *Mog*, *Mag*, *Mbp*, and *PLP1*; astrocytes, marked by *Glul*, *Slc1a3*, *Aqp4*, and *GAD2*; and endothelial cells, marked by *Fn1*, *Hmcn1*, and *Cped5*. As shown in Figure 1F-G, the distinct marker genes clearly delineate different clusters, and cells from all groups are evenly distributed across these clusters. These results confirm the successful integration of the four datasets and the accurate annotation of the corresponding cell types.

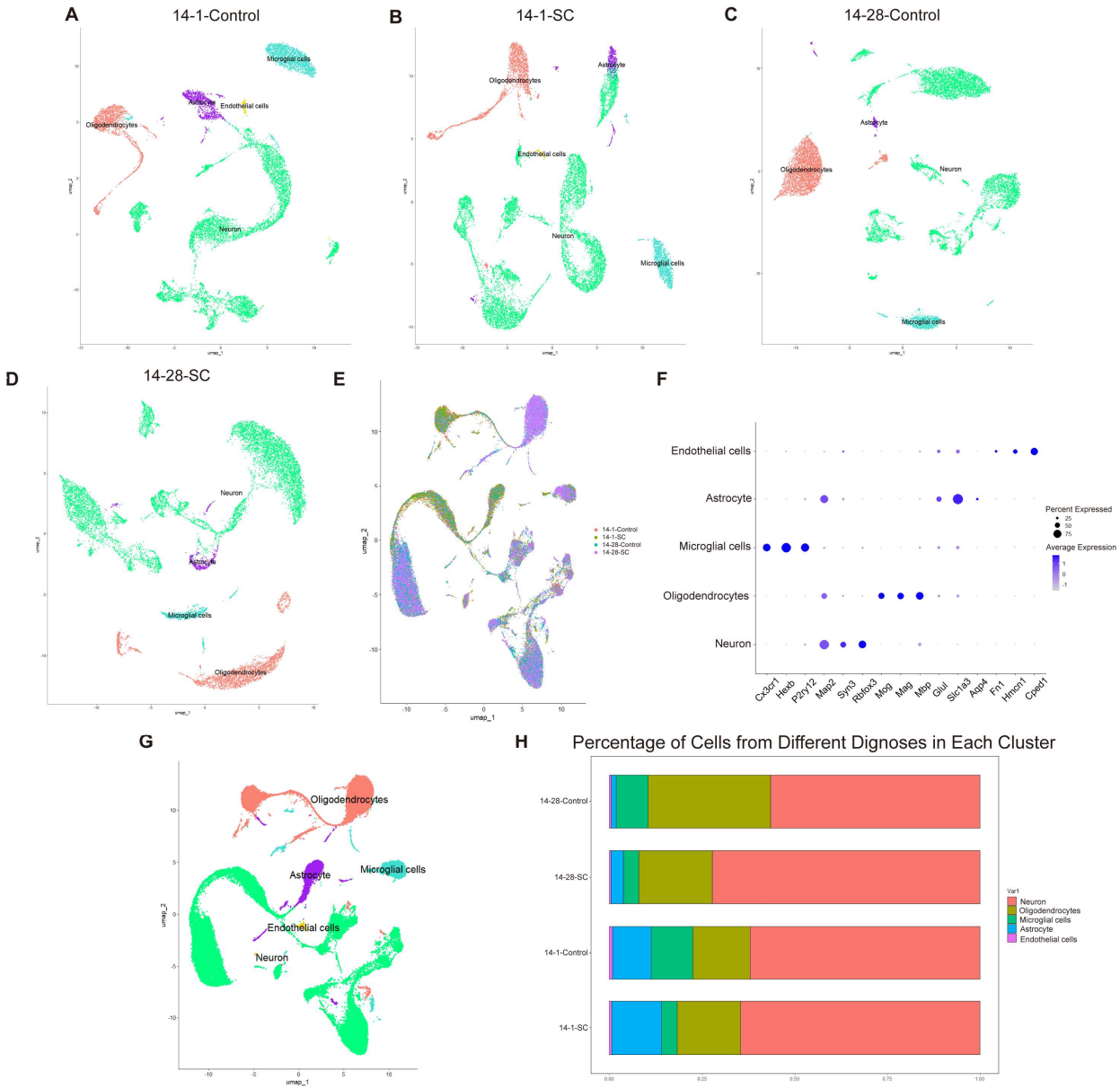


Figure 1. snRNA-seq analysis in developmental mice after seizures. (**A**) UMAP visualization of the 14-1 Control group. (**B**) UMAP of 14-1-SC group. (**C**) UMAP of 14-28-Control group. (**D**) UMAP of 14-28-SC group. (**E**) UMAP distribution of cells, annotated by cohort. (**F**) Dot plot showing selected differentially expressed genes for each cluster. (**G**) UMAP distribution of cells, colored by major cell types. (**H**) Histogram illustrating the percentage of cells from different cell types across the four groups.

By comparing the distribution of cell types across different populations, we identified cell types that were differentially distributed in specific populations. The analysis of cell populations revealed significant differences between the normal immature brain group and disease groups. In all four immature brain groups, neurons were the predominant cell type, followed by a smaller proportion of dendritic cells. The distribution of cell types, including neurons, oligodendrocytes, microglia, astrocytes, and endothelial cells, varied across the 14-1-Control, 14-1-SC, 14-28-Control, and 14-28-SC groups (Figure 1H). Specifically, neurons constituted 62%, 64%, 57%, and 72% of cells, respectively; oligodendrocytes constituted 16%, 17%, 33%, and 20%; microglia constituted 11%, 4%, 8%, and 4%; astrocytes constituted 10%, 14%, 1%, and 3%; and endothelial cells constituted 0.8%, 0.5%, 0.5% and 0.4%.

3.2. The Pressure Profiles of Normal and Epileptic Subgroups of Microglia in the Immature Developing Brain Reveal the Functional Characteristics of GAB$_B$R-Relative Microglia

Microglia, as resident macrophages in the brain, play essential roles in monitoring the brain environment, phagocytosing dead or damaged neurons, and remodeling synapses during the pathological progression of epilepsy [31]. Notably, microglia are crucial in the onset and progression of immature brain diseases associated with epilepsy [32,33]. To investigate their function in both normal and epileptic immature brains, we further subdivided the microglial population into two subgroups, each characterized by distinct marker genes and transcription factors (Figure 2A–C). For instance, steady-state microglial subpopulations predominantly express Cx3cr1, P2ry12, and Tmem119, which are linked to immune surveillance [34–36]. Conversely, activated microglial subtypes primarily express Apoe, Cd40, and Arg1, which are associated with neuroinflammatory responses and have been implicated in disease pathology. These subtypes also contribute to synaptic pruning and the clearance of aging neurons and extracellular debris in epilepsy models [36–38].

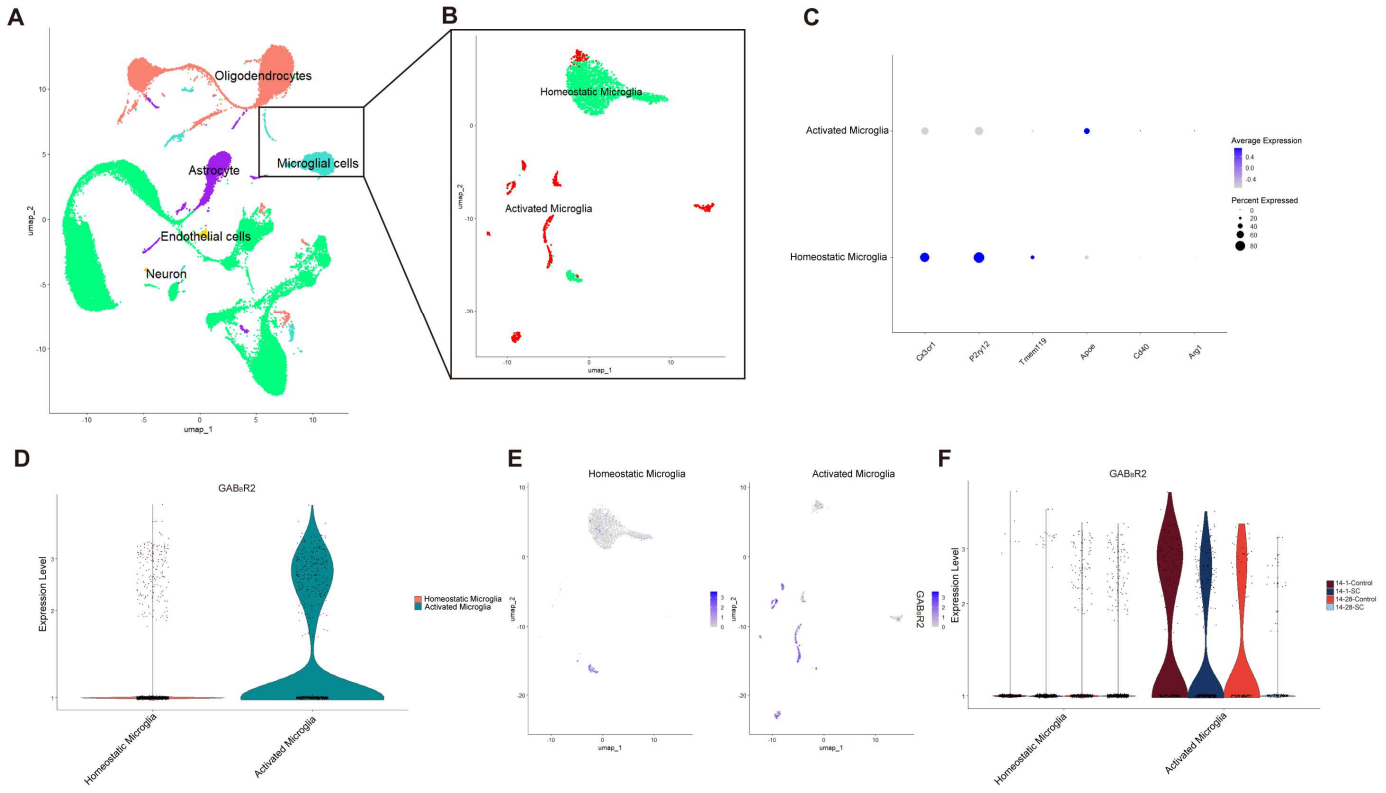


Figure 2. snRNA-seq analysis of GAB$_B$R-relative microglia in developmental mice. (**A**,**B**) The UMAP plot illustrates the reclustering of microglia into distinct subpopulations. (**C**) The dot plot highlights differentially expressed genes across clusters, with dot size indicating the proportion of nuclei expressing the gene in each cluster and color representing the mean expression level. (**D**) The violin plot visualizes the distribution of GAB$_B$R2 specific transcriptional feature scores across microglial subpopulations. (**E**) The UMAP plot depicts the spatial distribution of GAB$_B$R2 specific transcript expression, with the highest expression observed in activated microglia. (**F**) Another violin plot presents the distribution of GAB$_B$R2 specific transcriptional features across various microglial subgroups.

Next, we compared the expression of GAB$_B$R2 across different microglial subgroups. Interestingly, GAB$_B$R2 was predominantly expressed in activated microglia (Figure 2D,E), suggesting that its function in immature brains is closely linked to the activity of these cells. To further elucidate the expression trajectory of GAB$_B$R-associated microglia, we compared the expression levels of resting and activated microglia across four groups. Using the AddModulus Core method to calculate the GAB$_B$R2 expression score, we observed significant

differences in activated microglia between the 14-1-Control and 14-1-SC groups compared to the 14-28-Control and 14-28-SC groups (Figure 2F). Notably, GAB_BR2 expression was predominantly enriched in the 14-28-SC group, highlighting its potential regulatory role in the brains of chronic epilepsy models.

3.3. Decline in Cognitive and Learning Function in Chronic Epilepsy Mice

Emotional and cognitive disorders are commonly reported in epilepsy patients and corresponding mouse models [39–42]. This result focused on the cognitive and learning functions in epileptic mice during the chronic epilepsy phase post KA administration.

OFT was utilized to assess the spontaneous activity and exploratory behavior of mice. Results indicated that a notable decrease in both the number and duration of entries into the central area was observed, suggesting heightened anxiety in the unfamiliar environment (Figure 3A,B). In addition, compared to the control group, the total moving distance of epilepsy mice had no difference, indicating that there was no difference in motor ability between the two groups. (Figure 3B). EPM is a widely used behavioral test in research to assess anxiety-like behavior in mice. The findings revealed that compared to the control group, both the frequency and duration of entries into the open arms by chronic epilepsy mice were significantly reduced, indicating severe anxiety (Figure 3C,D).

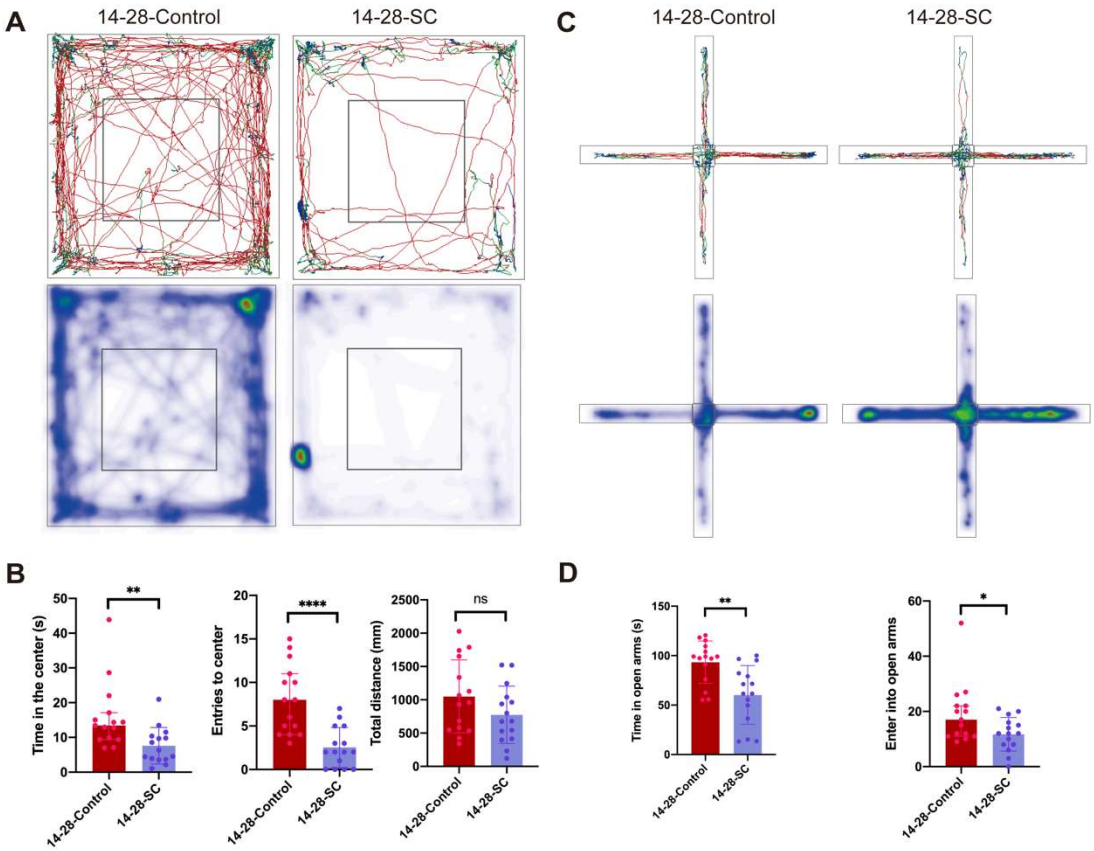


Figure 3. Detection of emotional changes of mice after intraperitoneal KA. (**A**) Representative track and heat maps of a 14-28-Control and a 14-28-SC mouse in the OFT. (**B**) 14-28-SC mouse spent significantly less time and entries in the center of OFT as compared to 14-28-Control group, but the total distance had no significant difference. (**C**) Representative track and heat maps of a 14-28-Control and a 14-28-SC mouse in the EPM. (**D**) Compared with the 14-28 control group, the test time and number of entries of the 14-28-SC group in the EPM open arm were significantly reduced. When compared with 14-28-Control group, ^{ns} $p > 0.05$, * $p < 0.05$, ** $p < 0.01$, and **** $p < 0.0001$; data are reported as the mean ± SD; unpaired two-tailed Student's *t*-test.

The NOR experiment was employed to assess learning and memory capabilities. Results indicated a decrease in the preference index for new objects in the 14-28-SC group compared to the 14-28-Control group (Figure 4A,B). Furthermore, the Y-maze test revealed a diminished alternation rate, suggesting impaired working memory in the epileptic mice. Additionally, a lower spontaneous alternation rate was observed in the 14-28-SC group compared to the 14-28-Control group (Figure 4C,D).

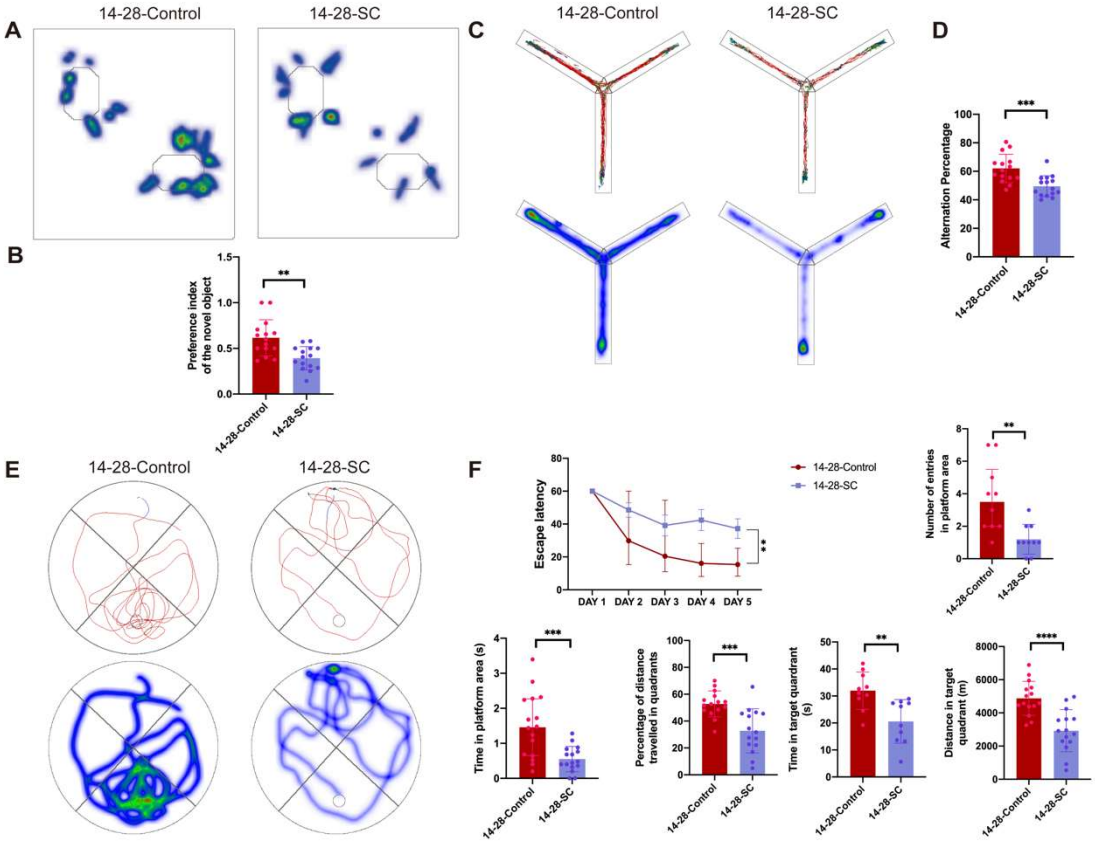


Figure 4. Detection of cognitive and learning function changes in mice after intraperitoneal KA. (**A**) Representative heat maps of a 14-28-Control and a 14-28-SC mouse in the NOR. (**B**) Compared to the 14-28-Control group, a decrease in the preference index for new objects in 14-28-SC group. (**C**) Representative track and heat chart of Y maze test. (**D**) Quantification of the alternation rate. (**E**) Representative track and heat maps of a 14-28-Control and a 14-28-SC mouse in the MWM. (**F**) Quantification of the escape latency, number of entries in the platform area, time in the platform area, percentage of distance traveled in quadrants, time in target quadrant and distance in the target quadrant. When compared with the 14-28-Control group, ** $p < 0.01$, *** $p < 0.001$ and **** $p < 0.0001$; data are reported as the mean ± SD; unpaired two-tailed Student's *t*-test.

Subsequently, the MWM test was conducted to evaluate the learning ability and spatial memory of chronic epileptic mice. During the training phase (over 5 consecutive days), epileptic mice spent more time searching for the platform than the control group, indicating that the learning ability of epileptic mice was impaired (Figure 4E,F). On the test day (day 6), metrics such as distance in the target quadrant, number of entries in the platform area, percentage of distance traveled in quadrants, time in the platform area, as well as time in the target quadrant were calculated. The 14-28-SC group crossed the platform area less frequently than the control group, indicating significant memory impairment (Figure 4F). Our findings suggest that chronic epileptic mice exhibit significant short-term learning and memory impairment. These results demonstrate that early seizures induce behavioral changes in developmental mice, manifesting as pronounced anxiety, depression, and learning and memory dysfunctions.

3.4. Expression and Distribution of GAB$_B$R-Relative Microglia After Epilepsy

To explore the role of GAB$_B$R-associated genes in epilepsy, we conducted a WB analysis on hippocampal tissues from control and epilepsy mouse groups aged 14–28 days. The results demonstrated a significant increase in GAB$_B$R2 protein expression in the 14-28-SC group (Figure 5A,B). Furthermore, qRT-PCR analysis revealed elevated GAB$_B$R2 mRNA levels in 14-28-SC group (Figure 5C).

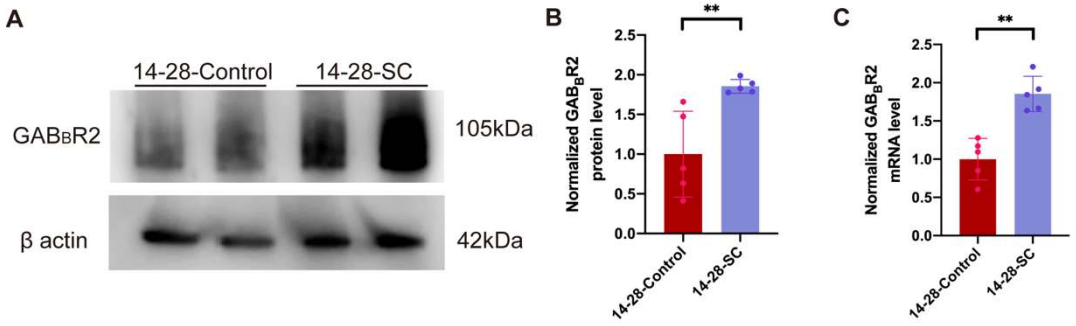


Figure 5. Expression of GABA$_B$2 after epilepsy. (**A**) Western blot analysis of GABA$_B$2 protein level in hippocampal samples from 14-28-Control and 14-28-SC mice. (**B**) Quantifications of GABA$_B$2 protein levels. (**C**) The mRNA level of GABA$_B$2 in 14-28-Control and 14-28-SC mice were detected by real-time PCR. ** $p < 0.01$; data are reported as the mean ± SD; unpaired two-tailed Student's *t*-test.

To investigate the relationship between GAB$_B$R-associated microglia and seizures, 14-day-old mice were selected for seizure induction via intraperitoneal injection of KA. Double immunofluorescence staining targeting microglia/GAB$_B$R-associated microglia markers IBA1 and GAB$_B$R2 was conducted in the hippocampus of both epileptic and control mice 1, 7, 14, and 28 days post injection. The distribution and density of GAB$_B$R-associated microglia in the mouse hippocampus were quantified using semi-quantitative immunofluorescence staining. There are no significant differences in the expression of GABAB-receptive microglia within the CA1, CA3, and DG regions of the hippocampus between control and epileptic groups at 1, 7 and 14 days early seizures in 14-day-old mice (Supplemental Figures S2–S4A,B). Results showed that the 14-28-SC group exhibited a significant increase in GAB$_B$R-associated microglia within the hippocampal CA1, CA3, and DG regions compared to the 14-28-Control group (Figure 6A,B). These findings suggest that although GAB$_B$R-associated microglia do not significantly influence acute seizure events in 14-day-old mice, they are implicated in the progression of chronic epilepsy.

3.5. Phagocytic Pruning Effect of GAB$_B$R-Receptive Microglia on Neurons After Chronic Epilepsy

Prior research has demonstrated a notable increase in the phagocytic activity of microglia towards neuronal synapses in the KA-induced epilepsy model [43,44]. To further explore the role of GAB$_B$R-associated microglia in early epileptic seizures in the developing mouse brain, we used immunofluorescence imaging combined with Imaris software to quantify neuronal content within microglia in the hippocampus of 14-28-Control and 14-28-SC mouse groups. The results revealed that GAB$_B$R-associated microglia in the hippocampus of the 14-28-SC group engulfed significantly more neurons compared to the control group (Figure 7A–C), indicating enhanced phagocytic activity. Additionally, morphological analysis showed that the richness, length, and number of terminal points of microglial branches associated with GAB$_B$R-associated were reduced in the 14-28-SC group compared to the control group (Figure 7D,E).

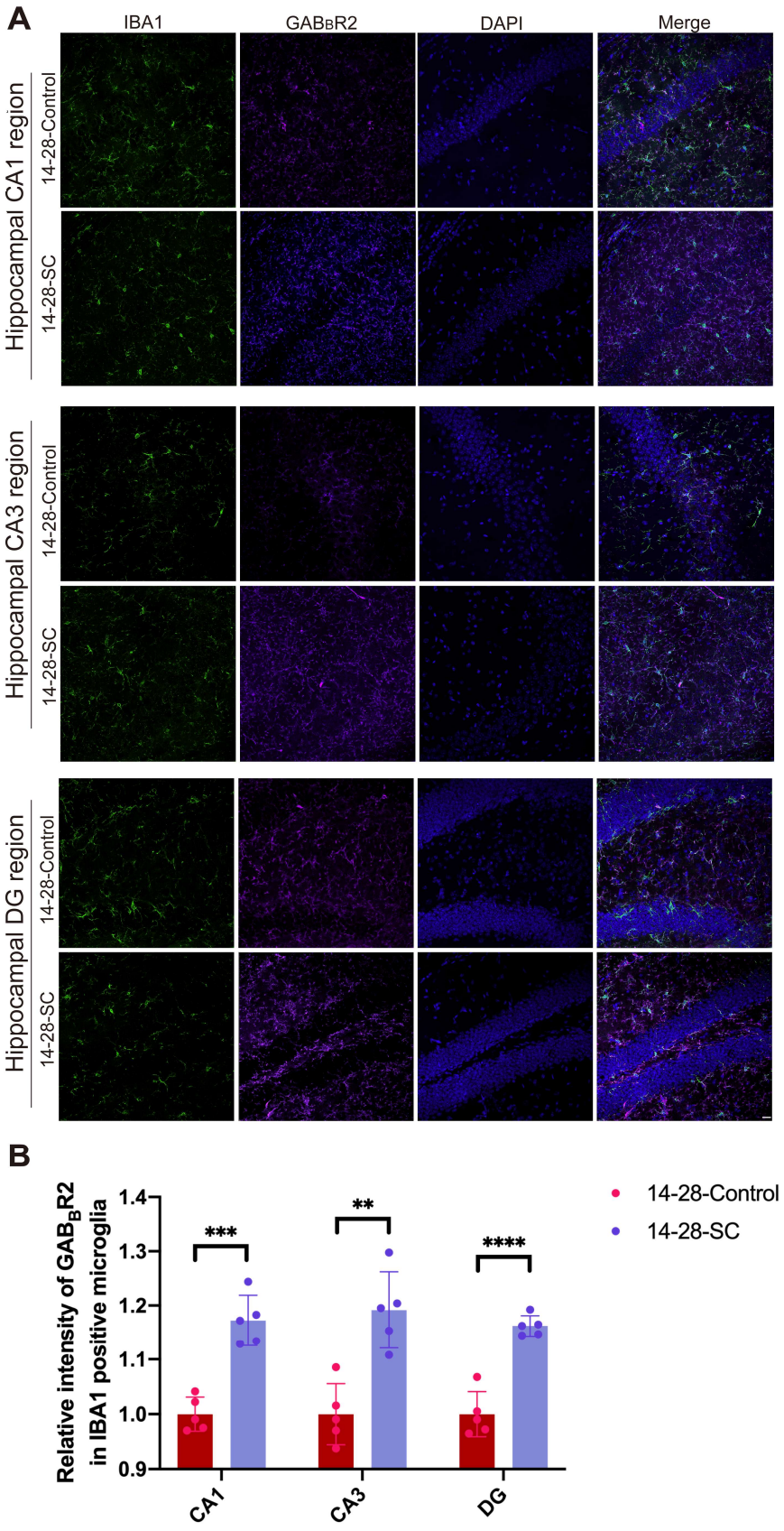


Figure 6. Distribution and expression of GAB_BR-relative microglia after epilepsy. (**A**) Immunofluorescent staining of GAB_BR2 and IBA1 of hippocampus CA1, CA3 and DG regions in 14-28-Control and 14-28-SC groups. Scale bars: 50 μm. (**B**) Quantifications of the percentage of $GAB_BR2^+/IBA1^+$ in the hippocampus CA1, CA3 and DG regions. ** $p < 0.01$, *** $p < 0.001$, and **** $p < 0.0001$; data are reported as the mean ± SD; unpaired two-tailed Student's *t*-test.

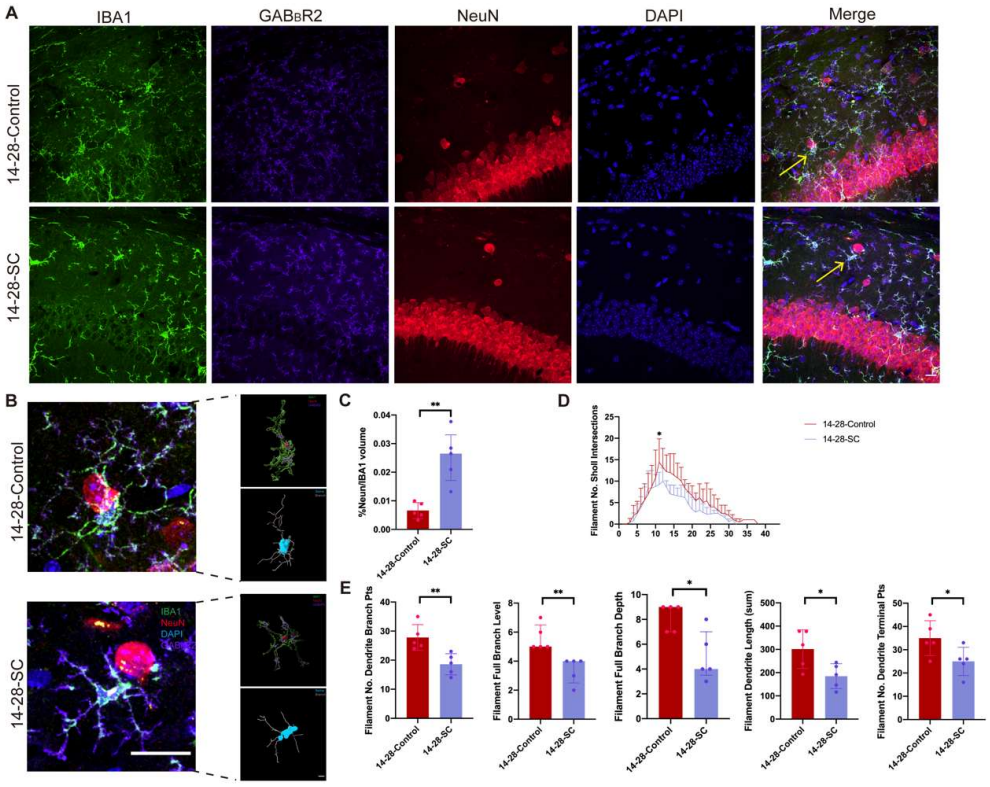


Figure 7. Phagocytic pruning effect of GAB_BR-relative microglia on neurons in epilepsy. (**A**) Immunofluorescent training for GAB_BR2 (purple), IBA1 (green) and NeuN (red) of hippocampus from 14-28-Control and 14-28-SC group. Arrows indicate 3D reconstructed GAB_BR-associated microglia. (**B**) Left: Immunofluorescent training for GAB_BR2, IBA1 and NeuN of hippocampus from 14-28-Control and 14-28-SC group. Scar bar: 30 μm. Right: IBA1/NeuN co-localization in Imaris and IBA1 morphology reconstruction in Imaris. Scar bar: 3 μm. (**C**) Quantifications of $IBA1^+NeuN$ colocalization using Surface module in Imaris. (**D**) Analysis of GAB_BR-associated microglial branch using Filament module in Imaris. Statistical analysis was performed using Two-Way ANOVA for (**D**). (**E**) Analysis of total branch, branch point count, terminal point count, branch depth, and branch level in GAB_BR-associated microglia using Filament module in Imaris. * $p < 0.05$; ** $p < 0.01$; data are reported as the mean ± SD; unpaired two-tailed Student's *t*-test.

These findings suggest that, in the 14-28-SC mouse model induced by intraperitoneal KA injection, GAB_BR-associated microglia exhibit not only heightened phagocytic activity toward neurons but also increased activation. Collectively, these results implicate GAB_BR-associated microglia in the phagocytic processes underlying the progression of chronic epilepsy.

4. Discussion

This study examined the alterations in the phagocytic function of GAB_BR-associated microglia in the brains of developing mice with a background of epilepsy, focusing on both acute and chronic epileptic seizures. A key innovation of this research is the application of single-nucleus RNA sequencing (snRNA-seq) to identify cellular subgroup differences in the brains of immature mice with acute and chronic epilepsy, specifically investigating GAB_BR2 expression within microglial subpopulations. Previous studies have primarily concentrated on the expression and role of GAB_BR-associated genes in epileptic neurons [45], leaving the functional role of these genes in microglia largely unexplored. This study indicates that, during the chronic phase following epileptic seizures in P14 mice, GAB_BR2 expression is significantly upregulated in activated microglia within the hippocampus. Notably, we also observed a pronounced increase in the phagocytic function

of GAB_BR-associated microglia in the brains of P14 mice during chronic epileptic seizures. These results highlight the potential importance of GAB_BR-associated microglia in the phagocytic mechanisms underlying chronic epileptic seizures.

The mechanisms underlying early-onset epilepsy differ significantly from those in mature brains. Childhood epilepsy can disrupt normal brain development and increase the risk of epilepsy later in life [46,47]. Consequently, understanding the pathogenesis of immature epilepsy in rodent models has become a critical area of research. Immature brains exhibit heightened excitability relative to inhibitory processes, resulting in an elevated risk of SE during early developmental stages [47,48]. The P0–P14 period in rodents corresponds to [49–51] the neonatal and infant stages of human brain development, making this developmental window ideal for modeling childhood epilepsy [33,48]. Administration of KA via intraperitoneal injection in young rodents (10–14 days old) induces SE and mimics key characteristics of childhood epilepsy in humans [33,52]. SRSs typically manifest by the third week following the induction of an epileptic state [49–51]. Our findings corroborate these observations, demonstrating significant SRS in KA-induced epilepsy models, which provide valuable insights into the pathogenesis of epilepsy in immature brains. Furthermore, cognitive and learning deficits have been documented in neonatal epilepsy models, highlighting the severe impact of these comorbidities on patients' quality of life [50,53–55]. It is worth noting that our rodent model of chronic immature epilepsy also exhibits emotional and cognitive impairments, underscoring the importance of neurological comorbidities as a focal point in epilepsy research.

Single-nucleus RNA sequencing (snRNA-seq) technology has significantly advanced the understanding of epilepsy pathogenesis in recent years [23,56]. By employing snRNA-seq to investigate the immune mechanisms underlying epilepsy, researchers have identified a synapse-associated trait formed by activated microglia and T cells in epileptic brain tissue [32]. Notably, due to developmental and site-specific variations, microglia may assume distinct roles in disease progression [57]. In epilepsy, pathological changes in the hippocampus are of particular interest, such as neuronal loss and gliosis [33]. In order to compare the gene expression patterns under steady-state and pathological conditions, we conducted snRNA-seq analysis on hippocampal tissue from mice. Our findings revealed widespread activation of microglia in the hippocampus of immature epilepsy model mice, with microglia transitioning toward a hyperactive, disease-associated phenotype. Previous studies suggest that activated microglia enhance their phagocytic activity following epileptic seizures, potentially mitigating the formation of hyperexcitable neural circuits [58,59]. However, the regulatory factors governing microglial phagocytic function during epilepsy [23,56] remain largely unexplored.

Gamma-aminobutyric acid (GABA) is the primary inhibitory neurotransmitter in the brain, crucial for transmitting inhibitory synaptic signals and maintaining the balance between excitation and inhibition (E/I balance) [60]. Recent studies have shown that GABA receptors, particularly GAB_BR, influence the functional mechanisms of microglia, facilitating bidirectional communication between neurons and microglia [12,61]. Also, some studies have also found that microglia mainly express GAB_BR subtype [17,62]. This result is consistent with the analysis of our study. Using hippocampal tissue isolated from 14-day-old mice, we categorized microglia into resting and activated states based on snRNA-seq data. In both types of cells, we observed that GAB_BR2 expression was markedly higher in activated microglia compared to resting microglia. Subsequently, a comparison of microglia during acute and chronic epilepsy revealed a significant increase in GAB_BR-expressing microglia during the chronic phase, while no notable changes were observed in the acute phase. The WB and IF experiments further validated this result. These findings are particularly relevant for understanding the role of GABA signaling in

the developing brain after epilepsy. Previous studies have shown that GABA enhances the activity of newly formed microglia through intrinsic GAB_BR signaling [62]. Based on the observed upregulation of GAB_BR2 in activated microglia, we propose that these cells enhance phagocytosis in the developing brain and may play a pivotal role in the pathophysiology of chronic epilepsy.

To verify this hypothesis, we analyzed morphological changes in GAB_BR-associated microglia within developing immature brains and their impact on neurons. Our findings reveal that, compared to the control group, GAB_BR-associated microglia in the epileptic hippocampus during development exhibit a more amoeboid morphology, indicative of increased activation. This suggests an enhancement in the phagocytic function of GAB_BR-associated microglia in the epilepsy group. Previous studies have shown that microglia engulf dead or damaged neurons or synapses [10,63]. During seizures, neuronal damage may result from excessive excitation or localized metabolic disturbances [64]. Microglia identify and clear these damaged neurons, thereby mitigating further brain injury [65,66]. This process helps protect the brain from further damage. In this study, it was found that there was a significant increase in neurons within GAB_BR-associated microglia in the epilepsy group, suggesting that GAB_BR facilitates the phagocytic activity of activated microglia toward neurons during chronic epileptic seizures. Thus, we propose that the heightened neuronal phagocytic activity of GAB_BR-associated microglia in the hippocampus may contribute significantly to the progression of immature brain disorders in the context of epilepsy.

In summary, our study emphasizes the phagocytic role of GAB_BR-associated microglia in the progression of developmental epilepsy. However, several limitations should be acknowledged. First, while we elucidated the phagocytic function of GAB_BR-associated microglia in immature brains, it remains unclear whether these microglia specifically target excitatory or inhibitory neurons. Second, previous studies on GAB_BR-associated microglia have shown their involvement in the remodeling of inhibitory synaptic connections [67]. Further research is required to elucidate the precise mechanisms through which GAB_BR-associated microglia contribute to epilepsy. Notably, the detailed snRNA-seq analysis conducted in this study provides valuable insights into the critical role of microglia in developmental epilepsy and offers new perspectives for the prevention and treatment of this condition.

5. Conclusions

GAB_BR-associated microglia significantly contribute to the progression of immature brain diseases by promoting neuronal phagocytic activity.

Supplementary Materials: The following supporting information can be downloaded at: https://www.mdpi.com/article/10.3390/biomedicines13020269/s1, Figure S1: Original Western blotting images of Figure 5; Figure S2: Distribution and expression of GABBR2 between 14-1-Control and 14-1-SC; Figure S3: Distribution and expression of GABBR2 between 14-7-Control and 14-7-SC; Figure S4: Distribution and expression of GABBR2 between 14-14-Control and 14-14-SC.

Author Contributions: Y.G. was a major contributor in performing experiments and writing the manuscript. Y.G., Z.H. and L.C. carried out the operation of tissue and related experiments. X.Y. and T.L. performed the tissue collection and analysis of the data. L.X. provided ideas for the experiments. L.J. designed the study and revised the manuscript. All authors have read and agreed to the published version of the manuscript.

Funding: This study was supported by grants from Doctoral Through Train Scientific Research Project of Chongqing (CSTB2022BSXM-JCX0041), the National Natural Science Foundation of China (NSFC

Grant 81701221), and Chongqing Natural Science Foundation General Project (CSTB2022NSCQ-MSX0809).

Institutional Review Board Statement: The animal study protocol was approved by the Animal Care and Committee of Chongqing Medical University (protocol code: IACUC-CQMU-2024-0639, approval date: July 28, 2024).

Informed Consent Statement: Not applicable.

Data Availability Statement: The datasets used and/or analyzed during the current study are available from the corresponding author on reasonable request. The raw data supporting the conclusions of this article will be made available by the authors, without undue reservation.

Conflicts of Interest: The authors declare that they have no competing interests.

References

1. Berg, A.T.; Berkovic, S.F.; Brodie, M.J.; Buchhalter, J.; Cross, J.H.; van Emde Boas, W.; Engel, J.; French, J.; Glauser, T.A.; Mathern, G.W.; et al. Revised terminology and concepts for organization of seizures and epilepsies: Report of the ILAE Commission on Classification and Terminology, 2005–2009. *Epilepsia* **2010**, *51*, 676–685. [CrossRef] [PubMed]
2. Jennum, P.; Pickering, L.; Christensen, J.; Ibsen, R.; Kjellberg, J. Morbidity and mortality of childhood- and adolescent-onset epilepsy: A controlled national study. *Epilepsy Behav.* **2017**, *66*, 80–85. [CrossRef]
3. Wirrell, E.; Wong-Kisiel, L.; Mandrekar, J.; Nickels, K. Predictors and course of medically intractable epilepsy in young children presenting before 36 months of age: A retrospective, population-based study. *Epilepsia* **2012**, *53*, 1563–1569. [CrossRef] [PubMed]
4. Trinka, E. What is the evidence to use new intravenous AEDs in status epilepticus? *Epilepsia* **2011**, *52* (Suppl. 8), 35–38. [CrossRef] [PubMed]
5. Symonds, J.D.; Elliott, K.S.; Shetty, J.; Armstrong, M.; Brunklaus, A.; Cutcutache, I.; Diver, L.A.; Dorris, L.; Gardiner, S.; Jollands, A.; et al. Early childhood epilepsies: Epidemiology, classification, aetiology, and socio-economic determinants. *Brain* **2021**, *144*, 2879–2891. [CrossRef] [PubMed]
6. Ali, A. Global Health: Epilepsy. *Semin. Neurol.* **2018**, *38*, 191–199. [CrossRef] [PubMed]
7. Owolabi, M.O.; Leonardi, M.; Bassetti, C.; Jaarsma, J.; Hawrot, T.; Makanjuola, A.I.; Dhamija, R.K.; Feng, W.; Straub, V.; Camaradou, J.; et al. Global synergistic actions to improve brain health for human development. *Nat. Rev. Neurol.* **2023**, *19*, 371–383. [CrossRef] [PubMed]
8. Koizumi, S.; Shigemoto-Mogami, Y.; Nasu-Tada, K.; Shinozaki, Y.; Ohsawa, K.; Tsuda, M.; Joshi, B.V.; Jacobson, K.A.; Kohsaka, S.; Inoue, K. UDP acting at P2Y6 receptors is a mediator of microglial phagocytosis. *Nature* **2007**, *446*, 1091–1095. [CrossRef]
9. Luo, L.; O'Leary, D.D. Axon retraction and degeneration in development and disease. *Annu. Rev. Neurosci.* **2005**, *28*, 127–156. [CrossRef] [PubMed]
10. Paolicelli, R.C.; Bolasco, G.; Pagani, F.; Maggi, L.; Scianni, M.; Panzanelli, P.; Giustetto, M.; Ferreira, T.A.; Guiducci, E.; Dumas, L.; et al. Synaptic pruning by microglia is necessary for normal brain development. *Science* **2011**, *333*, 1456–1458. [CrossRef]
11. Bosco, D.B.; Kremen, V.; Haruwaka, K.; Zhao, S.; Wang, L.; Ebner, B.A.; Zheng, J.; Xie, M.; Dheer, A.; Perry, J.F.; et al. Microglial TREM2 promotes phagocytic clearance of damaged neurons after status epilepticus. *Brain Behav. Immun.* **2024**, *123*, 540–555. [CrossRef]
12. Andoh, M.; Koyama, R. Microglia and GABA: Diverse functions of microglia beyond GABA-receiving cells. *Neurosci. Res.* **2023**, *187*, 52–57. [CrossRef]
13. Miller, M.W. GABA as a Neurotransmitter in Gastropod Molluscs. *Biol. Bull.* **2019**, *236*, 144–156. [CrossRef] [PubMed]
14. Sharma, P.; Sharma, B.S.; Raval, H.; Singh, V. Endocytosis of GABA receptor: Signaling in nervous system. *Prog. Mol. Biol. Transl. Sci.* **2023**, *196*, 125–139. [CrossRef] [PubMed]
15. Lujan, R.; Ciruela, F. GABAB receptors-associated proteins: Potential drug targets in neurological disorders? *Curr. Drug Targets* **2012**, *13*, 129–144. [CrossRef]
16. Gassmann, M.; Shaban, H.; Vigot, R.; Sansig, G.; Haller, C.; Barbieri, S.; Humeau, Y.; Schuler, V.; Müller, M.; Kinzel, B.; et al. Redistribution of GABAB(1) protein and atypical GABAB responses in GABAB(2)-deficient mice. *J. Neurosci.* **2004**, *24*, 6086–6097. [CrossRef] [PubMed]
17. Kuhn, S.A.; van Landeghem, F.K.; Zacharias, R.; Färber, K.; Rappert, A.; Pavlovic, S.; Hoffmann, A.; Nolte, C.; Kettenmann, H. Microglia express GABA(B) receptors to modulate interleukin release. *Mol. Cell. Neurosci.* **2004**, *25*, 312–322. [CrossRef]
18. Zhou, S.; Yu, Y. Synaptic E-I Balance Underlies Efficient Neural Coding. *Front. Neurosci.* **2018**, *12*, 46. [CrossRef]
19. Morin-Brureau, M.; Milior, G.; Royer, J.; Chali, F.; Le Duigou, C.; Savary, E.; Blugeon, C.; Jourdren, L.; Akbar, D.; Dupont, S.; et al. Microglial phenotypes in the human epileptic temporal lobe. *Brain* **2018**, *141*, 3343–3360. [CrossRef] [PubMed]

20. Ullal, G.; Fahnestock, M.; Racine, R. Time-dependent effect of kainate-induced seizures on glutamate receptor GluR5, GluR6, and GluR7 mRNA and Protein Expression in rat hippocampus. *Epilepsia* **2005**, *46*, 616–623. [CrossRef] [PubMed]
21. Racine, R.J. Modification of seizure activity by electrical stimulation. II. Motor seizure. *Electroencephalogr. Clin. Neurophysiol.* **1972**, *32*, 281–294. [CrossRef] [PubMed]
22. Xiong, Y.; Zhang, Y.; Zheng, F.; Yang, Y.; Xu, X.; Wang, W.; Zhu, B.; Wang, X. Expression of Glypican-4 in the brains of epileptic patients and epileptic animals and its effects on epileptic seizures. *Biochem. Biophys. Res. Commun.* **2016**, *478*, 241–246. [CrossRef] [PubMed]
23. Chen, Z.P.; Wang, S.; Zhao, X.; Fang, W.; Wang, Z.; Ye, H.; Wang, M.J.; Ke, L.; Huang, T.; Lv, P.; et al. Lipid-accumulated reactive astrocytes promote disease progression in epilepsy. *Nat. Neurosci.* **2023**, *26*, 542–554. [CrossRef]
24. Gulfo, M.C.; Lebowitz, J.J.; Ramos, C.; Hwang, D.W.; Nasrallah, K.; Castillo, P.E. Dopamine D2 receptors in hilar mossy cells regulate excitatory transmission and hippocampal function. *Proc. Natl. Acad. Sci. USA* **2023**, *120*, e2307509120. [CrossRef] [PubMed]
25. Lourenco, M.V.; Frozza, R.L.; de Freitas, G.B.; Zhang, H.; Kincheski, G.C.; Ribeiro, F.C.; Gonçalves, R.A.; Clarke, J.R.; Beckman, D.; Staniszewski, A.; et al. Exercise-linked FNDC5/irisin rescues synaptic plasticity and memory defects in Alzheimer's models. *Nat. Med.* **2019**, *25*, 165–175. [CrossRef]
26. Zhang, Y.; Wang, Z.; Wang, R.; Xia, L.; Cai, Y.; Tong, F.; Gao, Y.; Ding, J.; Wang, X. Conditional knockout of ASK1 in microglia/macrophages attenuates epileptic seizures and long-term neurobehavioural comorbidities by modulating the inflammatory responses of microglia/macrophages. *J. Neuroinflamm.* **2022**, *19*, 202. [CrossRef]
27. Leng, L.; Yuan, Z.; Pan, R.; Su, X.; Wang, H.; Xue, J.; Zhuang, K.; Gao, J.; Chen, Z.; Lin, H.; et al. Microglial hexokinase 2 deficiency increases ATP generation through lipid metabolism leading to β-amyloid clearance. *Nat. Metab.* **2022**, *4*, 1287–1305. [CrossRef]
28. Zhong, F.; Gan, Y.; Song, J.; Zhang, W.; Yuan, S.; Qin, Z.; Wu, J.; Lü, Y.; Yu, W. The inhibition of PGAM5 suppresses seizures in a kainate-induced epilepsy model via mitophagy reduction. *Front. Mol. Neurosci.* **2022**, *15*, 1047801. [CrossRef] [PubMed]
29. Charan, J.; Kantharia, N.D. How to calculate sample size in animal studies? *J. Pharmacol. Pharmacother.* **2013**, *4*, 303–306. [CrossRef]
30. Reid, M.M.; Kautzmann, M.I.; Andrew, G.; Obenaus, A.; Mukherjee, P.K.; Khoutorova, L.; Ji, J.X.; Roque, C.R.; Oria, R.B.; Habeb, B.F.; et al. NPD1 Plus RvD1 Mediated Ischemic Stroke Penumbra Protection Increases Expression of Pro-homeostatic Microglial and Astrocyte Genes. *Cell. Mol. Neurobiol.* **2023**, *43*, 3555–3573. [CrossRef]
31. Prinz, M.; Jung, S.; Priller, J. Microglia Biology: One Century of Evolving Concepts. *Cell* **2019**, *179*, 292–311. [CrossRef]
32. Kumar, P.; Lim, A.; Hazirah, S.N.; Chua, C.J.H.; Ngoh, A.; Poh, S.L.; Yeo, T.H.; Lim, J.; Ling, S.; Sutamam, N.B.; et al. Single-cell transcriptomics and surface epitope detection in human brain epileptic lesions identifies pro-inflammatory signaling. *Nat. Neurosci.* **2022**, *25*, 956–966. [CrossRef]
33. Rakhade, S.N.; Jensen, F.E. Epileptogenesis in the immature brain: Emerging mechanisms. *Nat. Rev. Neurol.* **2009**, *5*, 380–391. [CrossRef]
34. Masuda, T.; Sankowski, R.; Staszewski, O.; Böttcher, C.; Amann, L.; Sagar; Scheiwe, C.; Nessler, S.; Kunz, P.; van Loo, G.; et al. Spatial and temporal heterogeneity of mouse and human microglia at single-cell resolution. *Nature* **2019**, *566*, 388–392. [CrossRef]
35. Olah, M.; Menon, V.; Habib, N.; Taga, M.F.; Ma, Y.; Yung, C.J.; Cimpean, M.; Khairallah, A.; Coronas-Samano, G.; Sankowski, R.; et al. Single cell RNA sequencing of human microglia uncovers a subset associated with Alzheimer's disease. *Nat. Commun.* **2020**, *11*, 6129. [CrossRef]
36. Hammond, T.R.; Dufort, C.; Dissing-Olesen, L.; Giera, S.; Young, A.; Wysoker, A.; Walker, A.J.; Gergits, F.; Segel, M.; Nemesh, J.; et al. Single-Cell RNA Sequencing of Microglia throughout the Mouse Lifespan and in the Injured Brain Reveals Complex Cell-State Changes. *Immunity* **2019**, *50*, 253–271.e256. [CrossRef]
37. Patel, D.C.; Tewari, B.P.; Chaunsali, L.; Sontheimer, H. Neuron-glia interactions in the pathophysiology of epilepsy. *Nat. Rev. Neurosci.* **2019**, *20*, 282–297. [CrossRef]
38. Su, Y.; Zhou, Y.; Bennett, M.L.; Li, S.; Carceles-Cordon, M.; Lu, L.; Huh, S.; Jimenez-Cyrus, D.; Kennedy, B.C.; Kessler, S.K.; et al. A single-cell transcriptome atlas of glial diversity in the human hippocampus across the postnatal lifespan. *Cell Stem Cell* **2022**, *29*, 1594–1610.e1598. [CrossRef]
39. Song, X.; He, R.; Han, W.; Li, T.; Xie, L.; Cheng, L.; Chen, H.; Xie, M.; Jiang, L. Protective effects of the ROCK inhibitor fasudil against cognitive dysfunction following status epilepticus in male rats. *J. Neurosci. Res.* **2019**, *97*, 506–519. [CrossRef]
40. Mikulecká, A.; Druga, R.; Stuchlík, A.; Mareš, P.; Kubová, H. Comorbidities of early-onset temporal epilepsy: Cognitive, social, emotional, and morphologic dimensions. *Exp. Neurol.* **2019**, *320*, 113005. [CrossRef]
41. Ohgomori, T.; Jinno, S. Modulation of neuropathology and cognitive deficits by lipopolysaccharide preconditioning in a mouse pilocarpine model of status epilepticus. *Neuropharmacology* **2020**, *176*, 108227. [CrossRef] [PubMed]
42. Liu, H.; Stover, K.R.; Sivanenthiran, N.; Chow, J.; Cheng, C.; Liu, Y.; Lim, S.; Wu, C.; Weaver, D.F.; Eubanks, J.H.; et al. Impaired Spatial Learning and Memory in Middle-Aged Mice with Kindling-Induced Spontaneous Recurrent Seizures. *Front. Pharmacol.* **2019**, *10*, 1077. [CrossRef] [PubMed]

43. Akahoshi, N.; Murashima, Y.L.; Himi, T.; Ishizaki, Y.; Ishii, I. Increased expression of the lysosomal protease cathepsin S in hippocampal microglia following kainate-induced seizures. *Neurosci. Lett.* **2007**, *429*, 136–141. [CrossRef]
44. Banerjee, M.; Sasse, V.A.; Wang, Y.; Maulik, M.; Kar, S. Increased levels and activity of cathepsins B and D in kainate-induced toxicity. *Neuroscience* **2015**, *284*, 360–373. [CrossRef]
45. Minere, M.; Mortensen, M.; Dorovykh, V.; Warnes, G.; Nizetic, D.; Smart, T.G.; Hannan, S.B. Presynaptic hyperexcitability reversed by positive allosteric modulation of a GABABR epilepsy variant. *Brain* **2024**, awae232. [CrossRef]
46. Maytal, J.; Shinnar, S.; Moshé, S.L.; Alvarez, L.A. Low morbidity and mortality of status epilepticus in children. *Pediatrics* **1989**, *83*, 323–331. [CrossRef] [PubMed]
47. Raspall-Chaure, M.; Chin, R.F.; Neville, B.G.; Scott, R.C. Outcome of paediatric convulsive status epilepticus: A systematic review. *Lancet Neurol.* **2006**, *5*, 769–779. [CrossRef] [PubMed]
48. Dzhala, V.I.; Talos, D.M.; Sdrulla, D.A.; Brumback, A.C.; Mathews, G.C.; Benke, T.A.; Delpire, E.; Jensen, F.E.; Staley, K.J. NKCC1 transporter facilitates seizures in the developing brain. *Nat. Med.* **2005**, *11*, 1205–1213. [CrossRef]
49. Stafstrom, C.E.; Thompson, J.L.; Holmes, G.L. Kainic acid seizures in the developing brain: Status epilepticus and spontaneous recurrent seizures. *Brain Res. Dev. Brain Res.* **1992**, *65*, 227–236. [CrossRef]
50. Mikati, M.A.; Zeinieh, M.P.; Kurdi, R.M.; Harb, S.A.; El Hokayem, J.A.; Daderian, R.H.; Shamseddine, A.; Obeid, M.; Bitar, F.F.; El Sabban, M. Long-term effects of acute and of chronic hypoxia on behavior and on hippocampal histology in the developing brain. *Brain Res. Dev. Brain Res.* **2005**, *157*, 98–102. [CrossRef]
51. Sanchez, R.M.; Jensen, F.E. Maturational aspects of epilepsy mechanisms and consequences for the immature brain. *Epilepsia* **2001**, *42*, 577–585. [CrossRef]
52. Kubova, H.; Lukasiuk, K.; Pitkänen, A. New insight on the mechanisms of epileptogenesis in the developing brain. *Adv. Tech. Stand. Neurosurg.* **2012**, *39*, 3–44. [CrossRef] [PubMed]
53. Jensen, F.E.; Applegate, C.D.; Holtzman, D.; Belin, T.R.; Burchfiel, J.L. Epileptogenic effect of hypoxia in the immature rodent brain. *Ann. Neurol.* **1991**, *29*, 629–637. [CrossRef]
54. Koh, S.; Tibayan, F.D.; Simpson, J.N.; Jensen, F.E. NBQX or topiramate treatment after perinatal hypoxia-induced seizures prevents later increases in seizure-induced neuronal injury. *Epilepsia* **2004**, *45*, 569–575. [CrossRef] [PubMed]
55. Lin, J.J.; Mula, M.; Hermann, B.P. Uncovering the neurobehavioural comorbidities of epilepsy over the lifespan. *Lancet* **2012**, *380*, 1180–1192. [CrossRef]
56. Liu, Q.; Shen, C.; Dai, Y.; Tang, T.; Hou, C.; Yang, H.; Wang, Y.; Xu, J.; Lu, Y.; Wang, Y.; et al. Single-cell, single-nucleus and xenium-based spatial transcriptomics analyses reveal inflammatory activation and altered cell interactions in the hippocampus in mice with temporal lobe epilepsy. *Biomark. Res.* **2024**, *12*, 103. [CrossRef] [PubMed]
57. Wang, M.; Pan, W.; Xu, Y.; Zhang, J.; Wan, J.; Jiang, H. Microglia-Mediated Neuroinflammation: A Potential Target for the Treatment of Cardiovascular Diseases. *J. Inflamm. Res.* **2022**, *15*, 3083–3094. [CrossRef] [PubMed]
58. Dheer, A.; Bosco, D.B.; Zheng, J.; Wang, L.; Zhao, S.; Haruwaka, K.; Yi, M.H.; Barath, A.; Tian, D.S.; Wu, L.J. Chemogenetic approaches reveal dual functions of microglia in seizures. *Brain Behav. Immun.* **2024**, *115*, 406–418. [CrossRef]
59. Luo, C.; Koyama, R.; Ikegaya, Y. Microglia engulf viable newborn cells in the epileptic dentate gyrus. *Glia* **2016**, *64*, 1508–1517. [CrossRef]
60. Sears, S.M.; Hewett, S.J. Influence of glutamate and GABA transport on brain excitatory/inhibitory balance. *Exp. Biol. Med.* **2021**, *246*, 1069–1083. [CrossRef]
61. Liu, H.; Leak, R.K.; Hu, X. Neurotransmitter receptors on microglia. *Stroke Vasc. Neurol.* **2016**, *1*, 52–58. [CrossRef]
62. Logiacco, F.; Xia, P.; Georgiev, S.V.; Franconi, C.; Chang, Y.J.; Ugursu, B.; Sporbert, A.; Kühn, R.; Kettenmann, H.; Semtner, M. Microglia sense neuronal activity via GABA in the early postnatal hippocampus. *Cell Rep.* **2021**, *37*, 110128. [CrossRef]
63. Schafer, D.P.; Lehrman, E.K.; Kautzman, A.G.; Koyama, R.; Mardinly, A.R.; Yamasaki, R.; Ransohoff, R.M.; Greenberg, M.E.; Barres, B.A.; Stevens, B. Microglia sculpt postnatal neural circuits in an activity and complement-dependent manner. *Neuron* **2012**, *74*, 691–705. [CrossRef]
64. Shapiro, L.A.; Wang, L.; Upadhyaya, P.; Ribak, C.E. Seizure-induced Increased Neurogenesis Occurs in the Dentate Gyrus of Aged Sprague-Dawley Rats. *Aging Dis.* **2011**, *2*, 286–293.
65. Lewis, S. Development: Microglia go pruning. *Nat. Rev. Neurosci.* **2011**, *12*, 492–493. [CrossRef] [PubMed]
66. Hu, Y.; Yao, Y.; Qi, H.; Yang, J.; Zhang, C.; Zhang, A.; Liu, X.; Zhang, C.; Gan, G.; Zhu, X. Microglia sense and suppress epileptic neuronal hyperexcitability. *Pharmacol. Res.* **2023**, *195*, 106881. [CrossRef] [PubMed]
67. Favuzzi, E.; Huang, S.; Saldi, G.A.; Binan, L.; Ibrahim, L.A.; Fernández-Otero, M.; Cao, Y.; Zeine, A.; Sefah, A.; Zheng, K.; et al. GABA-receptive microglia selectively sculpt developing inhibitory circuits. *Cell* **2021**, *184*, 4048–4063.e4032. [CrossRef] [PubMed]

Disclaimer/Publisher's Note: The statements, opinions and data contained in all publications are solely those of the individual author(s) and contributor(s) and not of MDPI and/or the editor(s). MDPI and/or the editor(s) disclaim responsibility for any injury to people or property resulting from any ideas, methods, instructions or products referred to in the content.